Mononuclear phagocytes drive Mertk-dependent T cell regulation at autoimmune and tumor sites

Robin S. Lindsay[1,2], Kristen E. Dew[2+], Erika Rodriguez[2+], Jennifer C. Whitesell[1,2+], Dayna Tracy[2], Adam M. Sandor[1,2], Seth F. Yannacone[2], Jordan Jacobelli[2,1], Rachel S. Friedman*[2,1]

[1]Department of Immunology & Microbiology, University of Colorado Anschutz Medical Campus, Aurora, CO

[2]Department of Biomedical Research, National Jewish Health, Denver, CO

[+]Contributed equally

*Corresponding Author: Rachel S. Friedman, FriedmanR@NJHealth.org

Abstract

Understanding mechanisms of immune regulation is key to developing effective immunotherapies for autoimmunity and cancer; however, many regulatory mechanisms have not been elucidated. By analyzing T cell motility and activation at the disease site as well as disease progression, we examined the role of mononuclear phagocytes in driving regulation of effector T cells in type 1 diabetes and melanoma. We report that mononuclear phagocytes in the islets impair T cell responsiveness to antigen by preventing antigen-mediated T cell arrest. Mononuclear phagocytes in the autoimmune lesion express the TAM family receptor tyrosine kinase Mertk which functions in efferocytosis. Inhibition or deficiency of Mertk led to a release from T cell regulation characterized by enhanced T cell arrest in pre-diabetic islets and at the tumor site. This T cell arrest was accompanied by increased T cell-antigen presenting cell interactions as well as increased antigen experience and effector function by T cells in the islets. Notably, the effect of Mertk inhibition on T cell regulation was only seen at the disease site in the islets, not in draining lymph nodes. Inhibition of Mertk-dependent T cell regulation culminated in the rapid acceleration of autoimmune pathology and disease. In human islets, the number of Mertk-expressing cells were increased in remaining insulin-containing islets from type 1 diabetic patients, suggesting that they might have a protective role in human disease. These data indicate that Mertk signaling in mononuclear phagocytes drives T cell regulation that functions specifically at the disease site in peripheral tissues through a mechanism that prevents T cell arrest and response to antigen.

Introduction

Mechanisms of immune regulation function at all stages of the immune response to maintain and restore self-tolerance. These checkpoints provide layers of protection to control a normal immune response following pathogen clearance and to protect normal tissues from autoimmune destruction. These mechanisms of immune regulation also have the side effect of protecting many tumors from the immune response. The importance of understanding the multiple layers of immune regulation is highlighted by the fact that only 18%-36% of cancer patients respond to the targeting of a single checkpoint molecule (Hodi et al., 2010; Topalian et al., 2012) and response rates are improved by targeting multiple checkpoint molecules (Larkin et al., 2015). Thus, altering immune regulation for therapeutic purposes is likely to involve multiple pathways in most cancer and autoimmune patients.

Many layers of immune tolerance must be broken before autoimmune pathology occurs.

Type 1 diabetes (T1D) is largely caused by the T cell mediated autoimmune destruction of the pancreatic islets. We have shown that the T cell response in the islets is temporally regulated. Antigenic restimulation of T cells occurs in early stages of islet infiltration leading to pathogenic T cell effector function, followed by suppression of T cell pathogenesis as islet infiltration advances (Friedman et al., 2014; Lindsay et al., 2015). This T cell regulation in the islets eventually fails in mice that present with overt T1D. The mechanisms that drive this temporally controlled regulation of T cell pathogenesis at the disease site in the islets are still mostly unknown. This period of T cell regulation is important, because it could represent a novel tolerance checkpoint in the islets during T1D progression. Establishing and maintaining tolerance in the islets following infiltration is a critical step towards halting disease progression after the autoimmune response has been initiated. Understanding the mechanism by which T cells are regulated in the islets during advanced infiltration must be accomplished before we can target this pathway to therapeutically protect tissues from ongoing autoimmune attack.

This period of T cell regulation in advanced infiltrated islets is associated with a loss of antigen-mediated T cell arrest and transient rather than sustained interactions with antigen presenting cells (APCs) (Friedman et al., 2014; Lindsay et al., 2015) . T cell arrest and sustained T cell interactions with APCs are generally associated with antigen recognition and T cell stimulation, while T cell regulation or tolerance are associated with a lack of T cell arrest and with transient T cell-APC interactions (Hugues et al., 2004; Jacobelli et al., 2013; Katzman et al., 2010; Shakhar et al., 2005). For example, T cell tolerance through prevention of antigen-mediated T cell arrest has been shown to be mediated by factors such as regulatory T cells (Tadokoro et al., 2006; Tang et al., 2006) and co-inhibitory pathways including the PD-1 pathway (Fife et al., 2009). Notably, we have shown that, in the RIP-mOva model of T1D, blockade of PD-1 is insufficient to restore antigen-mediated T cell arrest in advanced insulitis (Friedman et al., 2014). Thus, the mechanism by which T cells are suppressed in the islets during advanced stages of infiltration is unknown.

Mononuclear phagocytes play a key role in the induction of T1D and its pathogenesis, but their role in modulating the immune response in the pancreatic islets during T1D is less clear. CD11c-depletion studies indicate that CD11c+ populations have a role in driving disease at early stages of T1D, while at later stages CD11c+ cells may slow disease progression (Saxena et al., 2007). This dichotomy could be due to temporal changes in CD11c+ populations, and/or differing roles of CD11c+ cells in different tissue locations (i.e. pancreatic lymph node vs. islets). The requirement for BatF3-dependent dendritic cells for the initial break in T cell tolerance in the draining pancreatic lymph nodes explains the requirement for CD11c+ cells prior to insulitis (Ferris et al., 2014; Gagnerault et al., 2002; Turley et al., 2003). CD11c+ cells also dramatically enhance entry of lymphocytes into inflamed islets, providing another potential node of disease regulation (Sandor et al., 2019). Yet, following the initial break in immunological tolerance the role of mononuclear phagocytes within the islets has not been elucidated. The fact that T1D progression is not altered by the removal of the draining

pancreatic lymph nodes following the establishment of insulitis (Gagnerault et al., 2002) suggests that the disease site in the islets may be the relevant site to interrogate. Resident and infiltrating mononuclear phagocytes are present in the islets during T1D, with the majority of both resident and infiltrating populations expressing CD11c (Calderon et al., 2015; Friedman et al., 2014; Jansen et al., 1994; Melli et al., 2009). Islet-resident mononuclear phagocytes are composed of macrophages and a minor population of CD103+ dendritic cells (Friedman et al., 2014; Yin et al., 2012), while islet-infiltrating mononuclear phagocytes are monocyte derived (Klementowicz et al., 2017). The function of the mononuclear phagocytes in the islets at different stages of islet infiltration is not clear.

Mertk, which is best known as a macrophage marker, is expressed on mononuclear phagocytes, and its signaling plays an immunoregulatory role in mononuclear phagocytes. Mertk is a member of the TAM family of receptor tyrosine kinases. TAM receptors and their ligands function in phagocytosis of apoptotic cells, tolerance induction, coagulation, and erythropoiesis (Lu and Lemke, 2001; Van Der Meer et al., 2014; Nagata et al., 1996; Nakano et al., 1997; Rothlin et al., 2015; Scott et al., 2001). Mertk-mediated apoptotic cell uptake results in immunoregulation of APCs to promote T cell tolerance (Wallet et al., 2008). In fact, Mertk has been implicated in T cell tolerance induction to self-antigens expressed by apoptotic beta cells in the NOD model (Wallet et al., 2008). It has been suggested that Mertk might be a checkpoint molecule that could be targeted to intervene in immune tolerance (Akalu et al., 2017; Cook et al., 2013), yet its role as such has not yet been clearly defined.

Having previously identified a transient regulation of T cells in T1D, we sought to identify the mediator of this immune tolerance checkpoint through interrogating the mechanism by which T cells are suppressed at the autoimmune disease site. Using *in vivo* imaging of the pancreatic islets, we found that CD11c+ cells prevent T cells from arresting and responding to their antigen via a Mertk-dependent mechanism. This result was mirrored in a solid tumor model, indicating the broad applicability of this mechanism. Mertk inhibition or deficiency drove increased T cell

arrest and increased sustained interactions of T cells with CD11c+ antigen-presenting cells. This led to a very rapid increase in antigen experience and lytic potential by islet-infiltrating T cells, which was restricted to the disease site. The increased T cell activation in the islets resulted in the rapid onset of type 1 diabetes in animals with pre-existing insulitis. Increased numbers of Mertk-expressing cells were also observed in the remaining intact islets of type 1 diabetes patients. These data indicate that Mertk signaling in mononuclear phagocytes is driving tissue protective T cell regulation specifically at the autoimmune and tumor disease site.

Results

CD11c+ cells mediate the suppression of T cell arrest in the islets.

We previously identified temporally controlled periods of T cell stimulation and suppression in the islets (Friedman et al., 2014; Lindsay et al., 2015). Advanced stages of islet infiltration were dominated by T cell regulation characterized by: a loss of antigen-mediated T cell arrest, pathogenic cytokine production, and interactions with CD11c^{+} cells (Friedman et al., 2014; Lindsay et al., 2015). Since dendritic cells (DCs), macrophages, and monocytes all have the potential to drive T cell tolerance, we hypothesized that a subset of CD11c+ cells drives this T cell regulation in advanced infiltrated islets. To test this hypothesis, we generated mixed bone marrow (BM) chimeras using NOD.CD11c-DTR (diphtheria toxin receptor) BM with either fluorescent islet-antigen specific 8.3 CD8 T cells (Fig 1A-H, Movie S1) or fluorescent polyclonal NOD T cells (Fig 1I-L). 5-10% fluorescently-labeled T cells were used to enable tracking of individual T cells. The chimeric mice were treated with two doses of diphtheria toxin (DT) to deplete the CD11c+ cells or vehicle (PBS) as a control. Forty-eight hours after the initial treatment, islets were isolated and imaged by 2-photon microscopy (Fig 1A,I). We have previously validated that this method of explanted imaging recapitulates T cell behavior in islets within the intact pancreas of live animals (Lindsay et al., 2015). The infiltration state of each islet analyzed was quantified to ensure that equivalent islets were analyzed in the intact and CD11c-depleted conditions (Fig 1C), since T cell behavior varies with the level of T cell infiltration (Friedman et al., 2014; Lindsay et al., 2015).

The depletion of CD11c+ cells resulted in significantly decreased islet antigen specific 8.3 CD8 T cell crawling speed within the islets (Fig 1B,D-E, Movie S1). The reduced crawling speed resulted in significantly reduced T cell translocation from the point of origin, as indicated by the mean squared displacement over time (Fig 1F). Furthermore, the 8.3 T cells in the islets

showed greater arrest as indicated by an increased arrest coefficient (% of time a T cells spends crawling <1.5μm/min) (Fig 1G). There was also a highly significant increase in the frequency of T cells with an arrest coefficient of 100, indicating that they were arrested for the entirety of the analysis period (Fig 1H). Notably, we previously determined that T cell arrest in the islets is antigen dependent and is correlated with increases in both T cell-APC interactions and T cell effector functions in the islets (Friedman et al., 2014; Lindsay et al., 2015), suggesting that the depletion of islet CD11c+ cells may be promoting T cell restimulation.

To determine whether CD11c+ cells have a similar effect on the motility and arrest of endogenous polyclonal CD4 and CD8 T cells in the islets, we depleted CD11c+ cells in mice with fluorescently-labeled polyclonal T cells (Fig 1I). The average T cell crawling speed (Fig 1J) and average T cell arrest coefficient (Fig 1K) were not significantly different between the CD11c-depleted and intact mice. This suggests that the CD11c+ cell dependent change in islet T cell motility is dependent on islet-antigen specificity. While not significant, the increase in fully arrested T cells (arrest coefficient of 100) following CD11c+ cell depletion (Fig 1L), suggests that a subset of islet-antigen specific CD8 T cells are also responding to CD11c+ cell depletion.

These data suggest that in the absence of suppressive CD11c+ cells, CD8 T cells are able to respond to antigen presented by other cells in the islets, such as beta cells, CD11c^{-} macrophages, or B cells, resulting in T cell arrest. The reduced effect on polyclonal T cells at a population level is likely due to the presence of non-islet antigen specific T cells in the islets and also the inability of CD4 T cells to recognize antigen on MHC class II^{-} beta cells. These data indicate that CD11c+ cells play a dominant role in preventing T cell arrest on APCs and target beta cells in the islets.

DCs can have the potential to be either stimulating or tolerogenic. We next sought to determine whether Zbtb46-expressing classical DCs within the islets were responsible for regulating T cell arrest. Since Zbtb46-DTR mice backcrossed to the NOD background are not available, we chose to use the RIP-mOva system in which a membrane bound form of

ovalbumin (mOva) is expressed in the beta cells under the rat insulin promoter (RIP). We generated bone marrow chimeras using B6.Zbtb46-DTR (Meredith et al., 2012) bone marrow transferred into irradiated C57BL/6.RIP-mOva recipients (Fig S1A). In this system the transfer of ovalbumin-specific OT-I CD8 T cells induces T cell infiltration of the islets (Kurts et al., 1997). Notably, our previous work has shown that islet-antigen specific OT-I T cells in RIP-mOva islets show the same dynamics of response as islet-antigen specific CD4 and CD8 T cells in the islets of NOD mice, including a period of T cell suppression in advanced infiltrated islets (Friedman et al., 2014). T cell infiltration of the islets was induced in the RIP-mOva.Zbtb46-DTR chimeric mice by transfer of naïve OT-I.Ubiquitin-GFP T cells. Three to five days following OT-I T cell transfer, the chimeric mice were treated with two doses of diphtheria toxin (DT) to deplete classical DCs or two doses of vehicle (PBS) as a control. Forty-eight hours after the initial dose, islets were isolated and imaged by 2 photon microscopy (Fig S1A). No differences were seen in the islet-antigen specific T cell crawling speed (Fig S1B) or arrest (Fig S1C) following classical DC depletion, despite equivalent infiltration of the islets analyzed (Fig S1D). These data indicate that classical DCs are not required for the T cell regulation mediated by CD11c+ cells in the islets.

Mertk is expressed on islet CD11c+ cells.

Since CD11c+ cell-mediated T cell regulation was not dependent on classical DCs, we sought to understand the source of the regulation in macrophage and monocyte populations. Monocyte-derived CD11c+ cells infiltrate the islets with T cells (Jansen et al., 1994; Klementowicz et al., 2017; Melli et al., 2009). Mertk is expressed on macrophages and some monocytes in peripheral tissues (Guilliams et al., 2014; Tamoutounour et al., 2013), mediates immunoregulation of APCs, and has been implicated in T cell tolerance in the NOD model (Cabezón et al., 2015; Cook et al., 2013; Wallet et al., 2008).

We previously identified CX3CR1 levels as a marker to distinguish resident CD11c+ cells from infiltrating CD11c+ cells (Friedman et al., 2014). Here we show that in NOD islets, the numbers of islet-infiltrating CX3CR1^{low} CD11c+ cells directly correlate with total levels of islet infiltration (Fig 2A-C). Mertk is expressed on both islet-resident (CX3CR1^{high}) and islet-infiltrating (CX3CR1^{low}) CD11c+ cells in the NOD model (Fig 2A-B,D) and Mertk-expressing CD11c+ cells increase with increasing islet infiltration (Fig 2E). Thus, based on the increased frequency of Mertk-expressing CD11c+ cells in advanced infiltrated islets, we sought to determine if Mertk signaling was responsible for driving T cell regulation.

Mertk regulates T cell arrest and T cell-APC interactions in the islets.

To test the hypothesis that Mertk signaling promotes T cell regulation in infiltrated islets, we treated mice orally with UNC2025, a highly selective inhibitor of Mertk and Flt3 (Zhang et al., 2014). T cell motility, arrest, and interactions with CD11c+ cells in the islets of UNC2025 or vehicle treated mice were analyzed. To ensure that UNC2025 was not reducing the CD11c+ or Mertk+ population in the islets via Flt3 inhibition, Mertk inhibition, or off-target effects, we analyzed the frequency of CD11c+ APCs and Mertk-expressing CD11c+ APCs in the islets following 4 weeks of continuous twice daily oral treatment with 30 μg/g of UNC2025. There was no significant difference in these populations following 4 weeks of treatment (Fig S2), thus we extrapolate that UNC2025 is not altering the frequency of the CD11c populations in the islets following short-term treatment.

To determine the effect of Mertk signaling on T cell regulation, we co-transferred fluorescently-labeled islet antigen specific 8.3 CD8 T cells and BDC-2.5 CD4 T cells into NOD.CD11c-mCherry hosts. These recipient mice were then treated with UNC2025 or vehicle for 17 hours and then isolated islets were imaged by 2-photon microscopy (Fig 3A, Movie S2). Notably, T cells do not express Mertk, thus Mertk-dependent T cell changes are likely to be extrinsically mediated by Mertk-expressing CD11c+ cells in the islets. The UNC2025 and

vehicle treated islets analyzed were matched for level of infiltration (Fig 3C). Following UNC2025 treatment, a highly significant decrease in both CD8 and CD4 T cell crawling speed and increase in T cell arrest was observed (Fig 3B,D-H,K-O, Movie S2), much like the islet-antigen specific T cell behavior we observed following CD11c+ cell depletion. The motility of the CD8 and CD4 T cells was more confined following UNC2025 treatment, as determined by the mean squared displacement, which is a readout of the T cell's ability to translocate away from its point of origin (Fig 3E-F,L-M). CD8 and CD4 T cells were also significantly more arrested in the islets following UNC2025 treatment (Fig 3G,N). Notably, there was a highly significant increase in CD8 T cells that were fully arrested (arrest coefficient of 100) and a highly significant decrease in T cells that were consistently motile (arrest coefficient of $\leq$10) following UNC2025 treatment (Fig 3H,O). These data suggest that Mertk inhibition by UNC2025 treatment can enable T cells to respond to their antigen in the islets.

Previous work has suggested that Mertk-dependent tolerance is mediated by modulation of costimulation, including CD40, CD80, and CD86 (Wallet et al., 2008). We find that these costimulatory ligands and PD-L1 are not modulated on CD11c+ cells by inhibition of Mertk (Fig S3), suggesting an alternative mechanism of T cell regulation. Thus, we next explored if prevention of interactions between T cells and APCs might be a possible mechanism of Mertk mediated regulation.

To determine whether T cell-APC interactions in the islets were increased as a result of Mertk inhibition, we analyzed 8.3 CD8 T cell and BDC-2.5 CD4 T cell interactions with CD11c+ cells following 17h of UNC2025 treatment. In the lymph nodes, brief T cell-APC interactions have been shown to be tolerogenic; whereas sustained T cell-APC interactions have been shown to be activating (Jacobelli et al., 2013). Thus, we analyzed the duration of T cell-CD11c+ cell interactions and the frequency of sustained interactions longer than 10 minutes in duration. Islet-antigen specific CD8 and CD4 T cells both showed a significant increase in the duration of interaction with CD11c+ APCs in the islets following UNC2025 treatment (Fig 3I,P). The

frequency of T cells with sustained CD11c+ cell interactions was also increased in CD8 T cells (Fig 3J,Q). These data suggest that Mertk inhibition may lead to an increase in antigen detection and T cell stimulation within the islets.

While the experiments using UNC2025 suggest that Mertk signaling is driving T cell regulation in the islets, effects on Flt3 signaling or off-target effects could contribute to this result. Thus, to confirm that T cell regulation in the islets is mediated by Mertk, we analyzed WT T cell motility in the islets of NOD.Mertk$^{-/-}$ mice. NOD.Mertk$^{-/-}$ mice have altered thymic selection which results in the absence of type 1 diabetes and strongly diminished spontaneous insulitis (Wallet et al., 2009). Thus, to induce islet infiltration, we transferred in vitro activated BDC-2.5 T cells into WT NOD and NOD.Mertk$^{-/-}$ recipients. Three to six days later, fluorescently labeled activated 8.3 CD8 T cells and BDC-2.5 CD4 T cells were transferred into the same hosts. Twenty-four hours after fluorescent T cell transfer, the islets were isolated and analyzed by 2-photon microscopy (Fig 4A-B, Movie S3). WT and Mertk$^{-/-}$ islets analyzed showed an equivalent amount of infiltration (Fig 4C). Islet-antigen specific CD8 and CD4 T cell motility was significantly reduced in the islets of Mertk$^{-/-}$ recipients compared to WT recipients (Fig 4D-E,I-J, Movie S3). The motility of the CD8 and CD4 T cells was also more confined in Mertk$^{-/-}$ islets, as determined by the mean squared displacement (Fig 4F,K). This was accompanied by a significant increase in T cell arrest in Mertk$^{-/-}$ islets (Fig 4G,L) with decreases in the frequency of fully motile T cells in the islets of Mertk$^{-/-}$ mice (Fig 4H,M). The pre-transfer of activated BDC-2.5 T cells was required to ensure our ability to analyze islets with matched infiltration in WT and Mertk$^{-/-}$ recipients; however, the resulting infiltration was not as advanced as in the islets analyzed with UNC2025 treatment. As a result, the overall T cell motility in WT recipients was lower, reducing the potential magnitude of differences upon arrest. The increased T cell arrest observed in Mertk$^{-/-}$ hosts suggests that the effects seen with UNC2025 result from the inhibition of Mertk signaling, and that Mertk signaling drives the T cell-extrinsic regulation of T cell arrest in infiltrated islets. These findings led to the question of whether this Mertk-mediated

mechanism of T cell regulation was specific to the pancreatic islets during type 1 diabetes or relevant to diverse disease settings.

Mertk regulates T cell arrest in a solid tumor.

TAM receptor family member mediated regulation of the T cell response within the tumor is an active area of clinical and pre-clinical research (Myers et al., 2019; Wu et al., 2018a). Mertk specific inhibition has been shown to suppress tumor growth in murine solid tumor models (Cook et al., 2013; Sinik et al., 2018; Wu et al., 2018b). Additionally, suppression of TAM receptor signaling has been shown to increase the response to anti-PD-1 therapy in a murine tumor model, suggesting that it is mediated by a mechanism other than PD-1 signaling (Kasikara et al., 2019), as we have observed in our autoimmune models. As a result, we sought to determine if similar inhibition of T cell motility within solid tumors was observed following Mertk inhibition.

To determine whether Mertk regulates T cell motility in a solid tumor setting, we analyzed T cell motility and arrest in B78ChOva tumors. We chose the B78ChOva tumor model because it has a high frequency of Mertk-expressing tumor associated macrophages and expresses ovalbumin (Broz et al., 2014). B78ChOva tumor cells were implanted subcutaneously in C57Bl/6 mice and allowed to grow for 4-6 days. Activated tumor-specific OT-I T cells were then transferred. Following T cell trafficking to the tumor site, mice were treated with either saline or UNC2025 for 18h. Tumors were then excised and imaged by 2 photon microscopy (Fig 5A). To ensure that the effect was Mertk specific the experiments were repeated comparing WT and Mertk$^{-/-}$ hosts.

The tumor specific OT-I T cells showed a dramatic change in motility following Mertk inhibition (Fig 5B-G) or in Mertk$^{-/-}$ hosts (Fig 5H-L). As in advanced infiltrated islets, OT-I T cells on the surface of the tumor were highly motile despite an abundance of local cognate antigen. However, when Mertk signaling was inhibited or deficient, the T cells arrested (Fig 5, Movie S4).

Both the T cells and tumor were WT in origin, even in the Mertk-/- hosts. This indicated that host derived cells, likely Mertk-expressing tumor associated macrophages, were responsible for the changes in T cell behavior. We next asked whether the restoration of T cell arrest by Mertk inhibition also promoted T cell activation.

T cell antigen recognition and effector function are increased following Mertk inhibition.

To determine how Mertk inhibition affected antigen recognition and activation by T cells in the islets and lymph nodes, we analyzed expression of CD44 and CD62L by flow cytometry following 17h of UNC2025 treatment of NOD mice. Polyclonal CD8 and CD4 T cells in the islets showed a rapid and significant increase in antigen experience ($CD44^{high}CD62L^{-}$) following Mertk inhibition (Fig 6A), suggesting that the increased arrest and T cell-APC interactions seen with Mertk inhibition are driving increased TCR signaling in the islets. Notably, there was no significant difference in antigen experience in the draining pancreatic lymph nodes or non-draining inguinal lymph nodes (Fig 6A). Together these data suggest that Mertk signaling is functioning to suppress the T cell response by preventing antigen recognition specifically at the disease site in the islets.

To determine whether effector function was also increased by Mertk inhibition, we analyzed expression of granzyme B in CD8 T cells by flow cytometry following 17-24h of UNC2025 treatment of NOD mice. Polyclonal CD8 T cells in the islets showed a rapid and significant increase in the amount of granzyme B following Mertk inhibition (Fig 6B). As seen with antigen experience, there was no significant difference in granzyme B expression in the draining pancreatic lymph nodes or non-draining inguinal lymph nodes (Fig 6B), further indicating that Mertk signaling is acting specifically at the disease site in the pancreatic islets. Notably, only half of the mice showed an increase in CD8 T cell granzyme B, indicating that while the T cells in the islets of all mice show increases in antigen experience, other mechanisms of tolerance may be preventing the licensing of T cells to increase lytic potential.

Inhibition of Mertk signaling drives rapid type 1 diabetes induction in mice with existing islet infiltration.

To determine how inhibition of Mertk affects type 1 diabetes progression, we treated NOD mice with UNC2025 or saline vehicle for 17h and analyzed changes in islet infiltration by quantification of histological staining. The data show a rapid increase in the frequency and degree of islet infiltration after only 17h of Mertk inhibition (Fig 7A). We also treated mice twice daily with UNC2025 or vehicle for 14 days and monitored blood glucose levels for diabetes. We chose >20 week old female NOD mice because we reasoned that this cohort would have a high proportion of infiltrated islets, where Mertk might be driving T cell regulation. Additionally, we treated WT female C57Bl/6 mice with UNC2025 as an additional control to ensure that UNC2025 did not have direct beta cell toxicity. The data showed that Mertk inhibition by UNC2025 treatment rapidly induced diabetes in a subset of the NOD mice (Fig 7B). The rapid nature of disease onset suggests that Mertk is playing a critical role in regulating T cell pathogenesis in the islets during type 1 diabetes. Notably, as we observed with increased CD8 T cell lytic potential, disease induction only occurred in half of treated NOD mice, suggesting that additional tolerance mechanisms within the islets may be protecting some of the mice. This led us to the question of whether Mertk also functions in humans to protect islets from destruction.

Remaining intact islets of type 1 diabetes patients have increased numbers of Mertk-expressing cells.

We hypothesized that if Mertk protects islets during type 1 diabetes, we would see an increased number of Mertk-expressing cells in the remaining intact islets of type 1 diabetes patients. Thus, we used immunofluorescent staining of pancreatic sections from control and type 1 diabetic donors obtained from nPOD (network of pancreatic organ donors) to test this

hypothesis. Control and type 1 diabetic donors had a similar mean age and sex distribution (Control: 23.3-44 years, mean 33.1 years; T1D: 20.3-42 years, mean 31.3 years). The type 1 diabetes patients had long-standing disease of 12-20 years. Insulin-containing islets from type 1 diabetes patients showed a significant increase in the number of Mertk-expressing cells in the islets when compared to the islets of controls (Fig 7C-D). Patient islets were slightly, but not significantly smaller than control islets, thus when Mertk+ cell numbers were normalized to islet size, the significance of the difference between patient and control islets was enhanced (data not shown).Together these data suggest that Mertk drives T cell regulation in infiltrated islets that prevents antigen recognition, restimulation, and pathogenic effector functions in islet infiltrating T cells by inhibiting antigen-mediated T cell arrest at the disease site.

Discussion

In this study, we sought to determine the mechanism by which autoreactive T cells are regulated at the tissue site of disease. Our results indicate that, following inflammation, CD11c-expressing cells act to prevent antigen mediated T cell arrest. This mechanism of T cell regulation is not dependent upon classical dendritic cells. Instead, Mertk signaling in macrophages and/or monocytes prevents antigenic stimulation of local T cells by preventing T cell arrest in the islets in type 1 diabetes and at the tumor site. Inhibition of this Mertk-mediated mechanism of T cell regulation led to increased antigen experience and effector function by T cells at the autoimmune site, but not in draining lymph nodes. Ultimately, inhibition of Mertk-mediated tolerance led to the acceleration of autoimmune pathology and disease progression. Increased numbers of Mertk-expressing cells were also observed in the remaining intact islets of type 1 diabetes patients. These data indicate that Mertk signaling in mononuclear phagocytes drives T cell regulation that prevents T cell arrest and response to antigenic stimuli, and this mechanism functions specifically at the disease site in peripheral tissues.

Our previous work indicated that T cell stimulation in the autoimmune lesion is controlled by modulating antigen-mediated T cell arrest during disease progression (Friedman et al., 2014; Lindsay et al., 2015). In type 1 diabetes progression, mild insulitis was characterized by antigen-mediated T cell arrest and restimulation, while advanced insulitis was characterized by the loss of antigen-mediated T cell arrest and antigenic stimulation (Friedman et al., 2014; Lindsay et al., 2015). These data suggest that tolerogenic pathways are functioning to prevent antigen-mediated T cell arrest. In a variety of systems, T cell tolerance induction has been associated with a lack of T cell arrest and with transient T cell-antigen presenting cells interactions (Jacobelli et al., 2013). For example, prevention of antigen-mediated T cell arrest as a means of tolerance induction has been established for the PD-1 pathway (Fife et al., 2009), where PD-1 signaling dephosphorylates CD28 to prevent co-stimulation (Hui et al., 2017). Notably, we have

shown that blockade of PD-1 is insufficient to restore antigen-mediated T cell arrest in advanced insulitis (Friedman et al., 2014), and that PD-L1 expression is not altered by Mertk inhibition (Fig S3). While Mertk signaling is known to play a role in immune regulation (Cabezón et al., 2015; Van Der Meer et al., 2014; Scott et al., 2001; Wallet et al., 2009), it has not previously been implicated in driving tolerance by inhibiting antigen-mediated T cell arrest. Here we show that inhibition of or deficiency in Mertk leads to increased T cell arrest within T1D islets and at tumor sites.

Many mechanisms work in concert to maintain and restore self-tolerance. This might be in part why Mertk inhibition led to increased effector function and disease progression in only half of the mice treated. It is likely that other mechanisms of tolerance were able to compensate for Mertk in some of the subjects, preventing the increased effector function and islet destruction. Despite preventing increased effector functions, other tolerance mechanisms were unable to prevent restoration of T cell arrest in both the islets and tumor. The asynchronous nature of disease in the NOD model might also play into this dichotomy since our data suggest that Mertk is functioning specifically within infiltrated islets. Thus, the percentage of uninfiltrated islets, which will not be destroyed upon Mertk inhibition, might determine whether or not Mertk inhibition results in overt diabetes. Co-inhibitory molecules such as CTLA-4, PD-1 and LAG-3 (Ansari et al., 2003; Bettini et al., 2011; Keir et al., 2006; Luhder et al., 2000; Lühder et al., 1998) as well as Tregs also provide layers of tolerance in the progression of type 1 diabetes (Tang et al., 2004a; Tarbell et al., 2007; Tonkin and Haskins, 2009). These regulatory mechanisms have roles in both the draining lymph node and at the disease site (Bettini et al., 2011; Fife et al., 2009; Keir et al., 2006; Luhder et al., 2000; Lühder et al., 1998; Tang et al., 2004b; Tarbell et al., 2007; Tonkin and Haskins, 2009). The role of Mertk in driving T cell tolerance following well established inflammation at the disease site could make it of particular importance when considering mechanisms that are critical in targeting tolerance of established disease at the site of pathology. Our previous work shows that the environment, controls the

behavior of the T cell in the islets (Friedman et al., 2014), thus we hypothesize that Mertk signaling creates a regulatory milieu, perhaps through generation of soluble mediators such as cytokines.

T1D has been proposed to be a relapsing remitting disease (von Herrath et al., 2007; van Megen et al., 2017), thus the temporal regulation of T cell pathogenesis in the islets could represent relapsing and remitting phases of disease within individual islets. Cycles of Mertk signaling initiation in the presence of β cell apoptosis followed by cessation once the autoimmune β cell destruction is controlled could control cycles of quiescent T cell tolerance followed by destructive re-initiation of T cell pathogenesis.

In this study, we identified Mertk signaling as a key mechanism in driving T cell regulation within the pancreatic islets during type 1 diabetes and at the tumor site. It is known that Mertk deficiency can also result in a systemic, lupus-like autoimmune phenotype (Scott et al., 2001). However, we would posit that this pathway is likely to inhibit antigen-mediated T cell arrest and stimulation in peripheral tissues under many conditions including other types of tissue specific autoimmunity and in other solid tumors. In fact, Mertk expression in tumor infiltrating macrophages has been implicated in enabling tumor growth and metastasis in MMTV-PyVmT and B16:F10 tumor models (Cook et al., 2013). In future studies it will be important to understand the breadth of function of this Mertk-dependent tolerance pathway, why it fails in autoimmune settings, and how it inhibits antigen-mediated T cell arrest.

Materials and Methods

Mice

NOD/ShiLtJ (Jackson 001976), NOD.8.3 (Jackson 005868), C57BL/6.RIP-mOva (Jackson 005431), C57BL/6.OT-I (Jackson 003831), C57BL/6.ZBTB46-DTR (Jackson 019506) and C57BL/6.Ubiquitin-GFP (Jackson 004353), C57BL/6.Mertk-/- (Jackson 011122) mice were obtained from The Jackson Laboratory and bred in-house. NOD.BDC-2.5 TCR transgenic [50], were a generous gift from the laboratory of Kathryn Haskins. NOD.CD11c-DTR [13] mice were a generous gift from the laboratory of Jonathan Katz. NOD.CD2-dsRed mice were a generous gift from the laboratory of Qizhi Tang. NOD.Mertk-/- mice were a generous gift from the laboratory of Roland Tisch. NOD.CX3CR1-GFP and NOD.CD11c-mCherry mice were generated by backcrossing for at least 10 generations. NOD.CX3CR1-GFP and NOD.CD11c-mCherry were confirmed to be fully backcrossed to our in house NOD mice utilizing speed congenic analysis performed by the Barbara Davis Center core facilities. All animal procedures were approved by the Institutional Animal Care and Use Committee at National Jewish Health.

Islet isolation

Islets were isolated as previously described [4,18]. Briefly mice were anesthetized with Ketamine/Xylazine prior to cervical dislocation. The pancreas was inflated via the common bile duct by adding ~3 ml of 0.8mg/ml Collagenase P (Roche) and 10µg/ml Dnase I (Roche) in HBSS (Cellgro). Following inflation the pancreas was removed and incubated at 37°C for 10-11 min and the islets were isolated by density centrifugation. The islets were handpicked under a dissecting microscope. For experiments in which islets were analyzed using flow cytometry single cell suspensions were generated by digestion with 0.4 Wunsch Units/ml Collagenase D (Roche) and 250 µg/ml DNAse I (Roche) in HBSS (Cellgro) with 10% FBS (Hyclone) at 37°C for

30 min. Following initial digestion islets were then incubated in Cell Dissociation Buffer (Sigma) at 37°C for an additional 30 min.

Tumor implantation and excision

$1x10^5$ B78ChOva tumor cells (generous gift of Max Krummel) were resuspended in PBS and mixed 1:1 with growth factor reduced Matrigel (Corning). Tumor cells were injected subcutaneously into each flank of WT or Mertk-/- C57BL/6 mice. At the time of harvest, tumors were carefully exposed by peeling the skin away from the peritoneum and excised with a border around the tumor. The skin associated with the tumor was affixed to a cover slip using VetBond (3M).

2-photon imaging of explanted islets and tumors

For 2 photon imaging, isolated islets were embedded in 3% low melting temperature agarose (Fisher) in DPBS. During imaging, islets and tumors were maintained at 35-37°C with flow of 95% O2/5% CO2 saturated RPMI (Gibco). Islets and tumors were imaged on an Olympus FV100MPE microscope as previously described [4,5]. Excitation was performed at 810nm for islets and 910nm for tumors. Imaging fields were as described [51], xy planes of 509 µm by 509 µm with a resolution of 0.994 µm/pixel were acquired. Images of 27- 53 xy planes with 3-um z-spacing were acquired every minute for 30 minutes. Four emission channels were used for data acquisition, blue (450- to 490-nm), green (500- to 550-nm), red (575- to 640-nm), and far-red (645- to 685-nm). In tumors collagen was imaged in the blue channel through second harmonic generation. The collagen was confirmed to be at the surface of the tumor by visualization of the mCherry tumor fluorescence at 810nm.

Image Analysis

Image analysis was performed using Imaris (Bitplane) and MATLAB (Mathworks). Images were linearly unmixed, as previously described [52]. Islet infiltration levels were determined as previous described [5]. Islets with similar levels of infiltration between groups were used for comparison. Cells in the islets that could be tracked for ≥5 min were used to obtain speed and average arrest coefficient (<1.5 µm/min cutoff for islets due to overall lower T cell speeds in the islets; <2 µm/min cutoff for tumors). Cells tracked for ≥10 min in the islets were used to determine mean squared displacement to ensure all cells analyzed could be included for all time points of the analysis. Interaction duration was calculated using a maximum distance between cells of 1 pixel (0.994 µm), with a minimum interaction of 2 timepoints to be defined as an interaction. Sustained interactions were defined as ≥10 min long interactions. Statistics were calculated with Prism software (GraphPad).

Activation and dye labeling of BD2.5, 8.3, and OT-I T cells

Spleen and lymph node cells from female BDC-2.5 or 8.3 mice or male/female OT-I.Ub-GFP mice were stimulated in vitro with 1µg/ml of BDC-2.5 mimetope (YVRPLWVRME) (Pi Proteomics), 1µg/ml of 8.3 peptide (KYNKANVEL) (Chi Scientific), or 100ng/ml of OT-I peptide (SIINFEKL) (Pi Proteomics). Beginning on day 2 post-activation, cells were maintained in media containing 10 IU/ml rhIL-2 (AIDS Research and Reference Reagent Program, Division of AIDS, NIAID, NIH from Dr. Maurice Gately, Hoffmann - La Roche Inc). Day 6-9 post-activation, BDC2.5 or 8.3 T cells were labeled with 1µM VPD (BD), 2 µM CFSE (Invitrogen), 20 µM CMTMR (Invitrogen), or 5µM eFluor670 (eBiosciences) for 25-30 minutes at 37°C. $1x10^7$ T cells were transferred intravenously into recipients with the timing indicated in the schematics provided for each experiment.

Generation and Treatment of BM Chimeras

<u>CD11c-DTR mixed BM chimeras</u>

Eight-week old WT NOD female mice were lethally γ-irradiated with 2 doses of 500 Rads. Following irradiation, 1x107 bone marrow cells (90% NOD.CD11c-DTR and 10% NOD.8.3.CD2-dsRed.CD11c-DTR or 95% NOD.CD11c-DTR and 5% NOD.CD11c-DTR.CD2-dsRed) were injected intravenously via the tail. Bone marrow chimeras were allowed to reconstitute for at least 8 weeks prior to use. Following reconstitution mice were injected with 2 doses of 200ng diphtheria toxin (Sigma) or control PBS 24 hours apart. Twenty-four hours after the final diphtheria toxin treatment islets were isolated and mounted for 2-photon imaging.

ZBTB46-DTR BM chimeras

C57BL/6.RIP-mOva mice were γ-irradiated with 2 doses of 500 Rads. Following irradiation, $1x10^7$ C57BL/6.ZBTB-46-DTR bone marrow cells were injected intravenously via the tail. Bone marrow chimeras were allowed to reconstitute for at least 8 weeks prior to use. C57BL/6.OT-I.Ubiquitin-GFP CD8+ T cells were enriched from single-cell suspensions of lymph nodes and spleens using mouse CD8-negative selection kits (Stem Cell Technologies). Enriched CD8 T cells ($5x10^6$) were injected into ZBTB-46-DTR-RIP-mOva bone marrow chimeras to induce islet infiltration. Two days prior to islet isolation, mice were treated with 2 doses of 200ng diphtheria toxin or control PBS 24 hours apart to deplete ZBTB-46 expressing cells. Day 5-7 post T cell transfer, islets were isolated for explanted imaging. Following islet isolation, T cell motility was assessed as by 2-photon imaging.

Flow Cytometry: Tissue preparation and Antibodies

Tissue isolation and digestion

Islets were isolated and digested as described above. Pancreatic (draining) or Inguinal (non-draining) lymph nodes were isolated and shredded using needles. Lymph nodes were

then digested with 0.4 Wunsch Units/ml Collagenase D (Roche) and 250 µg/ml DNAse I (Roche) in HBSS (Cellgro) with 10% FBS (Hyclone) at 37°C for 30 min.

Mertk identification panel

Islets were isolated from 4-18 week old NOD.CX3CR1-GFP+/- mice and dissociated as previously described. Islet samples were stained with fluorescent labeled antibodies (CD11c PE-Cy7 (Biolegend), MHCII PE (Biolegend), CD45 Pacblue (Biolegend)), unlabeled goat α-Mertk (R&D systems), and donkey α-goat secondary (AF647, Jackson Immuno)).

T cell activation panel

Isolated islet and lymph node cells were surface stained with CD45 BUV395 (BD), CD4 BV711 (Biolegend), CD8 APC-780 (eBioscience), CD62L Pacblue (Biolegend), CD44 FITC (Biolegend) for 30 minutes on ice.

Granzyme B intracellular panel

Isolated islet and lymph node cells were stained with fluorescent antibodies (CD45 BUV395 (BD), CD4 BV711 (Biolegend), CD8 FITC (Biolegend), dump PerCP-cy5.5 (CD11c (eBioscience), CD11b (Biolegend), Ter119 (BD), F4/80 (Biolegend), and CD19 (BD)) on ice for 30 minutes. Following surface staining, samples were fixed with 1% PFA (Sigma) and 3% sucrose (Sigma) for 13 minutes. Following fixation samples were stored overnight in permeabilization buffer (eBioscience). After overnight permeabilization, samples were stained intracellularly with Granzyme B (Pacblue, Biolegend) for 30 minutes at room temperature.

Flow Cytometry and Analysis

All samples were run on an LSR Fortessa (BD). Analysis and compensation were performed in FlowJo (TreeStar).

In vivo treatment with UNC2025

UNC2025 is a selective Mertk/Flt3 kinase inhibitor [36] that was initially developed to inhibit Mertk signaling in Mertk+ leukemia cells [36,53]. UNC2025 is orally bioavailable; however, it has a short half-life that requires twice daily dosing. UNC2025 (Meryx) was dosed at 30 mg/kg, which has been used to treat mice in a cancer setting [30,54]. Mice were treated twice daily for up to 4 weeks as indicated with daily monitoring of blood glucose and body weight.

Diabetes incidence

For disease incidence experiments all mice had normal glycemia prior to treatment. Blood glucose readings were taken daily prior to afternoon treatment. Mice with two consecutive readings >250 mg/dl were considered diabetic, and were euthanized. Mice were treated for at least 2 weeks unless sacrificed due to diabetes.

T cell activation

WT NOD 12-16 week old female mice were treated with 30 mg/kg UNC2025 or vehicle. Sixteen hours later mice were treated a second time with UNC2025 or vehicle. One hour after final treatment islets, draining pancreatic lymph node, and non-draining inguinal lymph node were harvested and digested as described above. Single cell suspensions were labeled with the T cell activation panel described above.

In vivo granzyme B

WT NOD 12-16 week old female mice were treated for 16 hours with UNC2025 or vehicle in the same manner as described above. At the same time a final UNC2025 treatment mice were injected intravenously with 250 µg of Brefeldin A (Sigma). Four hours after Brefeldin

A injection, islets, draining pancreatic lymph node, and non-draining inguinal lymph node were harvested. Samples were maintained in 10 µg/ml Brefeldin A on ice when possible until fixation. Islets and lymph nodes were digested and dissociated as described above. Staining was performed using the Granzyme B panel as described above. Due to changes in cytometer settings between experiments, mean fluorescent intensity (MFI) data were normalized for the purposes of graphing all experiments together. All samples were normalized to the average value of the vehicle controls from the same tissue in the same experiment. However, statistical analysis was performed on the data prior to normalization.

Islet section scoring

WT NOD female mice greater than 20 weeks of age were treated twice daily with 30mg/kg UNC2025 or vehicle. For islet sections, mice were treated twice 16 hours apart with UNC2025 or vehicle. One hour after the final treatment, the whole pancreas was excised and fixed in formalin (VWR) for 4 days. After fixation samples were stored in 70% ethanol until embedding in paraffin. Seven-µm sections were cut and fixed with Hematoxylin and Eosin. Embedding, sectioning and staining were performed by the University of Colorado Denver Anschutz histology core. Section scoring was performed blindly on a scale of 0 (no infiltration) to 4 (completely infiltrated).

Formalin-fixed paraffin embedded human pancreas sections were obtained from nPOD. Sections were deparaffinized using mixed xylenes (Sigma-Aldrich), and antigen retrieval was done using Tris pH10 antigen retrieval buffer in a pressure cooker for 10 minutes. Islets were stained for insulin (polyclonal guinea pig), CD3 (clone CD3-12), Mertk (clone Y323), and CD68 (clone KP1), all from Abcam. Secondaries included anti-GP-Cy3, anti-rat-DL649, anti-Mouse-biotin, anti-rabbit-biotin (all Donkey antibodies from Jackson Immuno) and Streptavidin-FITC, Streptavidin-BV421 (Biolegend). Mertk & CD68 stains were done sequentially with biotin-avidin blocking (Life Technologies) between stains. Differential staining patterns for CD68 and Mertk

confirmed successful blocking. Approximately 10 insulin-containing islets were imaged per donor using a Zeiss 710 confocal microscope. Islet images were analyzed in a blinded manner using Imaris software.

Analysis of UNC2025 treatment by imaging

Activated BDC-2.5 and 8.3 T cells were labeled with VPD or eFluor670 and transferred IV into 12-16 week old NOD.CD11c-mCherry female mice. Eight hours following T cell transfer mice were treated with 30 mg/kg UNC2025 or vehicle. Sixteen hours later mice were again treated with UNC2025 or vehicle. One hour later islets were isolated and imaged using our explanted imaging technique as previously described (explanted islet imaging).

Activated OT-I.Ub-GFP T cells were transferred into WT or Mertk-/- tumor bearing hosts 5-7 days before treatment. 18h prior to tumor harvest, mice were treated with 30 mg/kg UNC2025 or vehicle by oral gavage. Whole tumors were excised and mounted on cover slips for imaging. To ensure comparable microenvironments, tumor imaging was done in superficial regions of the tumor, where OT-I T cells were present, and the collagen rich tumor capsule was visible.

UNC2025 treated tissue explants were maintained in 50 μM UNC2025 for the duration of isolation and imaging. Imaging duration was 30 minutes long; image analysis was performed using Imaris and Matlab as previously described.

Analysis of T cell motility within Mertk-/- islets

For studies involving NOD.Mertk-/- mice, which do not spontaneously develop diabetes, islet infiltration was induced in NOD.Mertk-/- or control WT mice by transferring $1x10^7$ activated BDC-2.5 T cells 3-6 days prior to dye-labeled T cell transfer. Following initiation of islet infiltration $1x10^7$ VPD or eFlour670 dye labeled activated BDC2.5 and 8.3 T cells were transferred intravenously. Twenty-four hours following labeled T cell transfer islets were isolated

and imaged by 2-photon microscopy. Imaging duration was 30 minutes long; image analysis was performed using Imaris and Matlab as previously described.

Author Contributions

Conceptualization, R.S.F and R.S.L.; Methodology, R.S.F., R.S.L. and J.J.; Investigation, R.S.L., K.D., E.R., J.C.W., D.T., A.M.S., S.F.Y. and R.S.F.; Analysis, R.S.L., R.S.F., J.C.W., E.R. and J.J.; Writing – Original Draft, R.S.F. and R.S.L.; Writing –Review & Editing, R.S.F., R.S.L., A.M.S., J.C.W., and J.J.; Funding Acquisition, R.S.F.; Supervision, R.S.F.

Acknowledgements

We thank Meryx Inc. for providing UNC2025; Dr. Jonathan Katz, Dr. Katie Haskins, Dr. Qizhi Tang, and Dr. Roland Tisch for mice; Dr. Katie Haskins, Dr. John Cambier, Dr. Michael Holers, Dr. Ron Gill, Dr. Claudia Jakubzick, Dr. Ross Kedl, Dr. Rocky Baker, and Scott Thompson for guidance and helpful scientific input; Dr. Pippa Marrack, Dr. John Kappler, Dr. Ross Kedl, Dr. Claudia Jakubzick, Dr. Larry Wysocki, and Dr. Laurel Lenz for reagents; Robert Long, Matthew Gebert, Brianna Traxinger, Marlie Fisher, Katie Morgan, and Jessica Olivas, the National Jewish Health Flow Cytometry Core Facility, and the National Jewish Health Biological Resource Center for animal husbandry and technical assistance. This research was performed with the support of the Network for Pancreatic Organ donors with Diabetes (nPOD; RRID:SCR_014641), a collaborative type 1 diabetes research project sponsored by JDRF (nPOD: 5-SRA-2018-557-Q-R) and The Leona M. & Harry B. Helmsley Charitable Trust (Grant#2018PG-T1D053). Organ Procurement Organizations (OPO) partnering with nPOD to provide research resources are listed at http://www.jdrfnpod.org//for-partners/npod-partners/. This work was supported by funding from JDRF #2-2012-197 (RSF), the William & Ella Owens Medical Research Foundation (RSF), NIH 1R01DK111733-01 (RSF), George S. Eisenbarth nPOD Award from JDRF/Helmsley Trust (RSF), CRI #AWD-112499 (RSL).

Declaration of Interests

The authors declare no competing interests.

References

Akalu, Y.T., Rothlin, C. V., and Ghosh, S. (2017). TAM receptor tyrosine kinases as emerging targets of innate immune checkpoint blockade for cancer therapy. Immunol. Rev. *276*, 165–177.

Ansari, M.J.I., Salama, A.D., Chitnis, T., Smith, R.N., Yagita, H., Akiba, H., Yamazaki, T., Azuma, M., Iwai, H., Khoury, S.J., et al. (2003). The programmed death-1 (PD-1) pathway regulates autoimmune diabetes in nonobese diabetic (NOD) mice. J. Exp. Med. *198*, 63–69.

Bettini, M., Szymczak-Workman, A.L., Forbes, K., Castellaw, A.H., Selby, M., Pan, X., Drake, C.G., Korman, A.J., and Vignali, D.A.A. (2011). Accelerated Autoimmune Diabetes in the Absence of LAG-3. J. Immunol. *187*, 3493–3498.

Broz, M.L., Binnewies, M., Boldajipour, B., Nelson, A.E., Pollack, J.L., Erle, D.J., Barczak, A., Rosenblum, M.D., Daud, A., Barber, D.L., et al. (2014). Dissecting the Tumor Myeloid Compartment Reveals Rare Activating Antigen-Presenting Cells Critical for T Cell Immunity. Cancer Cell *26*, 638–652.

Cabezón, R., Carrera-Silva, E.A., Flórez-Grau, G., Errasti, A.E., Calderón-Gómez, E., Lozano, J.J., España, C., Ricart, E., Panés, J., Rothlin, C.V., et al. (2015). MERTK as negative regulator of human T cell activation. J. Leukoc. Biol. *97*, 751–760.

Calderon, B., Carrero, J.A., Ferris, S.T., Sojka, D.K., Moore, L., Epelman, S., Murphy, K.M., Yokoyama, W.M., Randolph, G.J., and Unanue, E.R. (2015). The pancreas anatomy conditions the origin and properties of resident macrophages. J. Exp. Med. *212*, 1497–1512.

Cook, R.S., Jacobsen, K.M., Wofford, A.M., DeRyckere, D., Stanford, J., Prieto, A.L., Redente, E., Sandahl, M., Hunter, D.M., Strunk, K.E., et al. (2013). MerTK inhibition in tumor leukocytes decreases tumor growth and metastasis. J. Clin. Invest. *123*, 3231–3242.

Ferris, S.T., Carrero, J.A., Mohan, J.F., Calderon, B., Murphy, K.M., and Unanue, E.R. (2014). A Minor Subset of Batf3-Dependent Antigen-Presenting Cells in Islets of Langerhans Is Essential for the Development of Autoimmune Diabetes. Immunity *41*, 657–669.

Fife, B.T., Pauken, K.E., Eagar, T.N., Obu, T., Wu, J., Tang, Q., Azuma, M., Krummel, M.F., and Bluestone, J. a (2009). Interactions between PD-1 and PD-L1 promote tolerance by blocking the TCR-induced stop signal. Nat. Immunol. *10*, 1185–1192.

Friedman, R.S., Lindsay, R.S., Lilly, J.K., Nguyen, V., Sorensen, C.M., Jacobelli, J., and Krummel, M.F. (2014). An evolving autoimmune microenvironment regulates the quality of effector T cell restimulation and function. Proc. Natl. Acad. Sci. U. S. A. *111*, 9223–9228.

Gagnerault, M.-C., Luan, J.J., Lotton, C., and Lepault, F. (2002). Pancreatic Lymph Nodes Are Required for Priming of Beta Cell Reactive T Cells in NOD Mice. J. Exp. Med. *196*, 369–377.

Guilliams, M., Ginhoux, F., Jakubzick, C., Naik, S.H., Onai, N., Schraml, B.U., Segura, E., Tussiwand, R., and Yona, S. (2014). Dendritic cells, monocytes and macrophages: a unified nomenclature based on ontogeny. Nat. Rev. Immunol. *14*, 571–578.

von Herrath, M., Sanda, S., and Herold, K. (2007). Type 1 diabetes as a relapsing-remitting disease? Nat. Rev. Immunol. *7*, 988–994.

Hodi, F.S., Day, S.J.O., Mcdermott, D.F., Weber, R.W., Sosman, J.A., Haanen, J.B., Gonzalez, R., Ph, D., Schadendorf, D., Hassel, J.C., et al. (2010). Improved survival with ipilimumab in patients with metastatic melanoma. N Engl J Med *363*, 711–723.

Hugues, S., Fetler, L., Bonifaz, L., Helft, J., Amblard, F., and Amigorena, S. (2004). Distinct T cell dynamics in lymph nodes during the induction of tolerance and immunity. Nat. Immunol. *5*, 1235–1242.

Hui, E., Cheung, J., Zhu, J., Su, X., Taylor, M.J., Wallweber, H.A., Sasmal, D.K., Huang, J., Kim, J.M., Mellman, I., et al. (2017). T cell costimulatory receptor CD28 is a primary target for PD-1–mediated inhibition. Science (80-.). *355*, 1428 LP – 1433.

Jacobelli, J., Lindsay, R.S., and Friedman, R.S. (2013). Peripheral tolerance and autoimmunity: lessons from in vivo imaging. Immunol. Res. *55*, 146–154.

Jansen, A., Homo-Delarche, F., Hooijkaas, H., Leenen, P.J., Dardenne, M., and Drexhage, H. a (1994). Immunohistochemical characterization of monocytes-macrophages and dendritic cells

involved in the initiation of the insulitis and beta-cell destruction in NOD mice. Diabetes *43*, 667–675.

Kasikara, C., Davra, V., Calianese, D., Geng, K., Spires, T.E., Quigley, M., Wichroski, M., Sriram, G., Suarez-Lopez, L., Yaffe, M.B., et al. (2019). Pan-TAM tyrosine kinase inhibitor BMS-777607 enhances anti-PD-1 mAb efficacy in a murine model of triple-negative breast cancer. Cancer Res. *79*, 2669–2683.

Katzman, S.D., O'Gorman, W.E., Villarino, A. V, Gallo, E., Friedman, R.S., Krummel, M.F., Nolan, G.P., and Abbas, A.K. (2010). Duration of antigen receptor signaling determines T-cell tolerance or activation. Proc. Natl. Acad. Sci. U. S. A. *107*, 18085–18090.

Keir, M.E., Liang, S.C., Guleria, I., Latchman, Y.E., Qipo, A., Albacker, L.A., Koulmanda, M., Freeman, G.J., Sayegh, M.H., and Sharpe, A.H. (2006). Tissue expression of PD-L1 mediates peripheral T cell tolerance. J. Exp. Med. *203*, 883–895.

Klementowicz, J.E., Mahne, A.E., Spence, A., Nguyen, V., Satpathy, A.T., Murphy, K.M., and Tang, Q. (2017). Origins, Recruitment, and Regulation of CD11c + Cells in Inflamed Islets of Autoimmune Diabetes Mice. J. Immunol. *199*, 27–32.

Kurts, B.C., Carbone, F.R., Barnden, M., Blanas, E., Allison, J., Heath, W.R., and Miller, J.F. a P. (1997). CD4+ T cell help impairs CD8+ T cell deletion induced by cross-presentation of self-antigens and favors autoimmunity. J. Exp. Med. *186*, 2057–2062.

Larkin, J., Chiarion-Sileni, V., González, R., Grob, J., Cowey, C., and Lao, C. (2015). Combined Nivolumab and Ipilimumab or Monotherapy in Previously Untreated Melanoma. N Engl J Med. 2015;373 23–34. *373*, 23–34.

Lindsay, R.S., Corbin, K., Mahne, A., Levitt, B.E., Gebert, M.J., Wigton, E.J., Bradley, B.J., Haskins, K., Jacobelli, J., Tang, Q., et al. (2015). Antigen recognition in the islets changes with progression of autoimmune islet infiltration. J. Immunol. *194*, 522–530.

Lu, Q., and Lemke, G. (2001). Homeostatic Regulation of the Immune System by Receptor Tyrosine Kinases of the Tyro 3 Family. Science (80-.). *293*, 306–311.

Luhder, F., Chambers, C., Allison, J.P., Benoist, C., and Mathis, D. (2000). Pinpointing when T cell costimulatory receptor CTLA-4 must be engaged to dampen diabetogenic T cells. Proc. Natl. Acad. Sci. U. S. A. *97*, 12204–12209.

Lühder, B.F., Höglund, P., Allison, J.P., Benoist, C., and Mathis, D. (1998). Cytotoxic T lymphocyte-associated antigen 4 (CTLA-4) regulates the unfolding of autoimmune diabetes. J. Exp. Med. *187*, 427–432.

Van Der Meer, J.H.M., Van Der Poll, T., and Van't Veer, C. (2014). TAM receptors, Gas6, and protein S: Roles in inflammation and hemostasis. Blood *123*, 2460–2469.

van Megen, K.M., Spindler, M.P., Keij, F.M., Bosch, I., Sprangers, F., van Royen-Kerkhof, A., Nikolic, T., and Roep, B.O. (2017). Relapsing/remitting type 1 diabetes. Diabetologia *60*, 2252–2255.

Melli, K., Friedman, R.S., Martin, A.E., Finger, E.B., Miao, G., Szot, G.L., Krummel, M.F., and Tang, Q. (2009). Amplification of autoimmune response through induction of dendritic cell maturation in inflamed tissues. J. Immunol. *182*, 2590–2600.

Meredith, M.M., Liu, K., Darrasse-Jeze, G., Kamphorst, a. O., Schreiber, H. a., Guermonprez, P., Idoyaga, J., Cheong, C., Yao, K.-H., Niec, R.E., et al. (2012). Expression of the zinc finger transcription factor zDC (Zbtb46, Btbd4) defines the classical dendritic cell lineage. J. Exp. Med. *209*, 1153–1165.

Myers, K. V., Amend, S.R., and Pienta, K.J. (2019). Targeting Tyro3, Axl and MerTK (TAM receptors): Implications for macrophages in the tumor microenvironment. Mol. Cancer *18*, 1–14.

Nagata, K., Ohashi, K., Nakano, T., Arita, H., Zong, C., Hanafusa, H., and Mizuno, K. (1996). Identification of the product of growth arrest-specific gene 6 as a common ligand for Axl, Sky, and Mer receptor tyrosine kinases. J. Biol. Chem. *271*, 30022–30027.

Nakano, T., Ishimoto, Y., Umeda, M., Inoue, K., Ohashi, K., and Mizuno, K. (1997). Cell Adhesion to Phosphatidylserine Mediated by a Product of Growth Cell Adhesion to Phosphatidylserine Mediated by a Product of Growth arrest-specific gene 6. J. Biol. Chem. *272*,

29411-4.

Rothlin, C. V., Carrera-Silva, E.A., Bosurgi, L., and Ghosh, S. (2015). TAM Receptor Signaling in Immune Homeostasis. Annu. Rev. Immunol. *33*, 355–391.

Sandor, A.M., Lindsay, R.S., Dyjack, N., Whitesell, J.C., Rios, C., Bradley, B.J., Haskins, K., Serreze, D. V., Geurts, A.M., Chen, Y.G., et al. (2019). CD11c + cells are gatekeepers for lymphocyte trafficking to infiltrated islets during type 1 diabetes. Front. Immunol. *10*, 1–17.

Saxena, V., Ondr, J.K., Magnusen, A., Munn, D., and Katz, J.D. (2007). The countervailing actions of myeloid and plasmacytoid dendritic cells control autoimmune diabetes in the nonobese diabetic mouse. J Immunol *179*, 5041–5053.

Scott, R.S., McMahon, E.J., Pop, S.M., Reap, E. a, Caricchio, R., Cohen, P.L., Earp, H.S., and Matsushima, G.K. (2001). Phagocytosis and clearance of apoptotic cells is mediated by MER. Nature *411*, 207–211.

Shakhar, G., Lindquist, R.L., Skokos, D., Dudziak, D., Huang, J.H., Nussenzweig, M.C., and Dustin, M.L. (2005). Stable T cell-dendritic cell interactions precede the development of both tolerance and immunity in vivo. Nat. Immunol. *6*, 707–714.

Sinik, L., Minson, K.A., Tentler, J.J., Carrico, J., Bagby, S.M., Robinson, W.A., Kami, R., Burstyn-Cohen, T., Eckhardt, S.G., Wang, X., et al. (2018). Inhibition of MERTK Promotes Suppression of Tumor Growth in BRAF Mutant and BRAF Wild-Type Melanoma. Mol. Cancer Ther. *18*, 278–288.

Tadokoro, C.E., Shakhar, G., Shen, S., Ding, Y., Lino, A.C., Maraver, A., Lafaille, J.J., and Dustin, M.L. (2006). Regulatory T cells inhibit stable contacts between $CD4^+$ T cells and dendritic cells in vivo. J. Exp. Med. *203*, 505–511.

Tamoutounour, S., Guilliams, M., Montanana Sanchis, F., Liu, H., Terhorst, D., Malosse, C., Pollet, E., Ardouin, L., Luche, H., Sanchez, C., et al. (2013). Origins and Functional Specialization of Macrophages and of Conventional and Monocyte-Derived Dendritic Cells in Mouse Skin. Immunity 925–938.

Tang, Q., Boden, E., Henriksen, K., Bour-Jordan, H., Bi, M., and Bluestone, J. (2004a). Distinct roles of CTLA-4 and TGF-beta in CD4+CD25+ regulatory T cell function. Eur. J. Immunol. *34*, 2996–3005.

Tang, Q., Henriksen, K.J., Bi, M., Finger, E.B., Szot, G., Ye, J., Masteller, E.L., McDevitt, H., Bonyhadi, M., and Bluestone, J.A. (2004b). In Vitro–expanded Antigen-specific Regulatory T Cells Suppress Autoimmune Diabetes. J. Exp. Med. *199*, 1455–1465.

Tang, Q., Adams, J.Y., Tooley, A.J., Bi, M., Fife, B.T., Serra, P., Santamaria, P., Locksley, R.M., Krummel, M.F., and Bluestone, J. a (2006). Visualizing regulatory T cell control of autoimmune responses in nonobese diabetic mice. Nat. Immunol. *7*, 83–92.

Tarbell, K. V, Petit, L., Zuo, X., Toy, P., Luo, X., Mqadmi, A., Yang, H., Suthanthiran, M., Mojsov, S., and Steinman, R.M. (2007). Dendritic cell-expanded, islet-specific CD4+ CD25+ CD62L+ regulatory T cells restore normoglycemia in diabetic NOD mice. J Exp Med *204*, 191–201.

Tonkin, D.R., and Haskins, K. (2009). Regulatory T cells enter the pancreas during suppression of type 1 diabetes and inhibit effector T cells and macrophages in a TGF-??-dependent manner. Eur. J. Immunol. *39*, 1313–1322.

Topalian, S., Hodi, F., Brahmer, J., Gettinger, S., Smith, D., McDermott, D., Powderly, J., Carvajal, R., Sosman, J., Atkins, M., et al. (2012). Safety, activity, and immune correlates of anti-PD-1 antibody in cancer. N Engl J Med. *366*, 2443–2454.

Turley, S., Poirot, L., Hattori, M., Benoist, C., and Mathis, D. (2003). Physiological beta cell death triggers priming of self-reactive T cells by dendritic cells in a type-1 diabetes model. J. Exp. Med. *198*, 1527–1537.

Wallet, M.A., Sen, P., Flores, R.R., Wang, Y., Yi, Z., Huang, Y., Mathews, C.E., Earp, H.S., Matsushima, G., Wang, B., et al. (2008). MerTK is required for apoptotic cell-induced T cell tolerance. J. Exp. Med. *205*, 219–232.

Wallet, M.A., Flores, R.R., Wang, Y., Yi, Z., Kroger, C.J., Mathews, C.E., Earp, H.S.,

Matsushima, G., Wang, B., and Tisch, R. (2009). MerTK regulates thymic selection of autoreactive T cells. Proc. Natl. Acad. Sci. U. S. A. *106*, 4810–4815.

Wu, G., Ma, Z., Cheng, Y., Hu, W., Deng, C., Jiang, S., Li, T., Chen, F., and Yang, Y. (2018a). Targeting Gas6/TAM in cancer cells and tumor microenvironment. Mol. Cancer *17*, 1–10.

Wu, J., Frady, L.N., Bash, R.E., Cohen, S.M., Schorzman, A.N., Su, Y.T., Irvin, D.M., Zamboni, W.C., Wang, X., Frye, S. V., et al. (2018b). MerTK as a therapeutic target in glioblastoma. Neuro. Oncol. *20*, 92–102.

Yin, N., Xu, J., Ginhoux, F., Randolph, G.J., Merad, M., Ding, Y., and Bromberg, J.S. (2012). Functional specialization of islet dendritic cell subsets. J. Immunol. *188*, 4921–4930.

Zhang, W., Deryckere, D., Hunter, D., Liu, J., Stashko, M.A., Minson, K.A., Cummings, C.T., Lee, M., Glaros, T.G., Newton, D.L., et al. (2014). UNC2025, a potent and orally bioavailable MER/FLT3 dual inhibitor. J. Med. Chem. *57*, 7031–7041.

Figure Legends:

Figure 1: CD11c+ cells in the islets prevent T cell arrest. NOD.CD11c-DTR bone marrow (BM) chimeras containing **(A-H)** 90% NOD.CD11c-DTR BM +10% NOD.CD11c-DTR.8.3.CD2-dsRed BM or **(I-L)** 95% CD11c-DTR + 5% CD11c-DTR.CD2-dsRed were treated twice with PBS (Control) or DT (CD11c depleted). **(A,I)** Schematic of experimental setup to analyze T cell motility in explanted islets by 2-photon microscopy. **(B)** Representative islet images from PBS control or DT treated mice with 10 minute tracks of motion. Dashed line depicts islet border. **(C)** Average level of islet infiltration. **(D,J)** Average T cell crawling speed per islet. **(E)** Representative 15 min tracks of motion of 15 randomly selected T cells. **(F)** Mean squared displacement over time indicates the T cells' ability to translocate away from their place of origin. **(G,H,K,L)** Arrest coefficient: % of time a T cell is moving <1.5 µm/min. **(A-L)** Data pooled from 3 independent experiments. Error bars represent SEM. **(A-H)** n = 10 islets from PBS treated mice and 11 islets from DT treated mice. **(I-L)** n = 13 islets from PBS treated mice and 15 islets from DT treated mice. **(C,D,G,J,K)** Statistics: Students T test. **(F)** Statistics: Two-way ANOVA. **(H,L)** Statistics: Multiple unpaired T tests with Holm-Sidak correction. **= $p<0.01$.

Figure 2: Mertk expressing cells increase with progression of islet infiltration. Islets from 4-18 week old NOD or NOD.CX3CR1-GFP female mice were isolated, digested and dissociated, stained, and analyzed by flow cytometry. **(A)** Example histograms of CX3CR1 gating in female NOD.CX3CR1-GFP islets. **(B)** Example plots of Mertk+CX3CR1^{Low} gating in female NOD islets. **(C-E)** Each dot represents one mouse, as the # of cells in the islets normalized to the # of islets per mouse. **(C)** Quantification of CD11c^{+}MHC-II^{+}CX3CR^{1ow} (infiltrating APCs) versus the leukocyte infiltration in the islets. **(D)** Quantification of CD11c+MHC-II+Mertk^{+} cells versus CX3CR1^{low} CD11c+MHC-II+ infiltrating APCs in the islets. **(E)** Mertk+CD11c+MHC-II+ versus leukocyte infiltration in the islets. **(A-D)** n=11 mice from 2

independent experiments. **(E)** n=24 mice from 6 independent experiments. **(C,D,E)** Statistics calculated by Pearson correlation.

Figure 3: Mertk signaling drives regulation of T cell arrest and interactions with APCs in the islets. Activated 8.3 CD8 T cells and BDC-2.5 CD4 T cells were fluorescently labeled and co-transferred into female NOD.CD11c-mCherry mice. Mice were treated twice daily with saline vehicle or 30 mg/kg UNC2025, a small molecule inhibitor of Mertk and Flt3. 17h following the initial treatment, islets were isolated and analyzed by 2-photon microscopy. **(A)** Schematic of experimental setup. **(B)** Representative islet images from vehicle or UNC2025 treated mice with 10 minute tracks of motion. **(C)** Average level of islet infiltration. **(D,K)** Average T cell crawling speed per islet. **(E,L)** Representative 15 min tracks of motion of 15 T cells. **(F,M)** Mean squared displacement over time indicates the T cells' ability to translocate away from their place of origin. **(G,H,N,O)** Arrest coefficient : % of time that a cell crawls <1.5µm/min. **(I,P)** Duration of T cell interactions with CD11c+ cells. **(J,Q)** % of T cell interactions with CD11c+ cells that last for ≥10 min. **(A-Q)** n = 6 islets from Vehicle treated mice and 9 islets from UNC2025 treated mice from 2 independent experiments. **(C,D,G,K,N)** Statistics: Two-tailed Student t test. Error bars: SEM. **(F,M)** Statistics: 2-way ANOVA with Bonferroni post-test. Error bars: SEM. **(H,O)** Statistics: Multiple unpaired T tests with Holm-Sidak correction. **p< 0.01, ***p< 0.001. **(I,J,P,Q)** Statistics: Unpaired t-test with Welch's correction. Box: 25th-75th percentiles, Line: median, Whisker: min-max.

Figure 4: Islet antigen-specific T cells in Mertk-/- islets show decreased motility and increased T cell arrest. Activated BDC-2.5 CD4 T cells were transferred into NOD or NOD.Mertk-/- female mice to initiate islet infiltration. Fluorescently labeled activated 8.3 CD8 and BDC-2.5 CD4 T cells were then transferred into the same mice 3-6 days later. Twenty-four hours after fluorescent T cell transfer, islets were isolated and analyzed by 2-photon

microscopy. **(A)** Schematic of experimental setup. **(B)** Representative islet images from WT NOD or NOD.Mertk-/- mice with 10 minute tracks of motion. Dashed line depicts islet border. **(C)** Average level of islet infiltration. **(D,I)** Average T cell crawling speed per islet. **(E,J)** Representative 15 min tracks of motion of 15 T cells. **(F,K)** Mean squared displacement over time. **(G,H,L,M)** Arrest coefficient: % of time that a cell crawls <1.5µm/min. **(C-M)** Data are pooled from 4-5 independent experiments. Error bars: SEM. **(D-H)** n= 22 WT and 23 Mertk-/- islets or **(I-M)** n= 25 WT and 28 Mertk-/- islets. **(C,D,G,I,L)** Statistics: Two-tailed Student t test. **(F,K)** Statistics: 2-way ANOVA with Bonferroni post-test. **(H,M)** Statistics: Multiple unpaired T tests with Holm-Sidak correction. **p< 0.01, ***p< 0.001.

Figure 5: Mertk signaling prevents T cell arrest in a solid tumor model. B78ChOva tumor cells were implanted in C57BL/6 or C57BL/6.Mertk-/- mice. Activated OT-I.Ub-GFP CD8 T cells were then transferred into tumor bearing mice mice 4-6 days later. Five to seven days after fluorescent T cell transfer, mice were treated with UNC2025 or vehicle. 18h after treatment, tumors were excised and analyzed by 2-photon microscopy. **(A)** Schematic of experimental setup. **(B)** Representative images of OT-I T cell (green) motility on the tumor surface with 10 minute tracks of motion. Collagen (blue) delineates the tumor surface. **(C,H)** Average T cell crawling speed in the tumor. **(D,I)** Representative 15 min tracks of motion of OT-I T cells. **(E,J)** Mean squared displacement over time. **(F,G,K,L)** Arrest coefficient: % of time that a cell crawls <2µm/min. **(B-L)** Data are pooled from 3-6 independent experiments. Error bars: SEM. **(B-L)** n= 10 WT, 6 UNC2025, and 5 Mertk-/- tumors. **(C,F,H,K)** Statistics: Two-tailed Student t test. **(E,J)** Statistics: 2-way ANOVA with Bonferroni post-test. **(G,L)** Statistics: Multiple unpaired T tests with Holm-Sidak correction. **p< 0.01.

Figure 6: T cell antigen experience and effector function increases specifically at the disease site in the islets following Mertk inhibition. (A-B) NOD female mice were treated

with UNC2025 or vehicle. Islets and lymph nodes were isolated 16h-24h post-treatment initiation, digested, stained and analyzed by flow cytometry. **(A)** Quantification of antigen experience by CD44/CD62L expression. Gated on $CD45^{+}CD90.2^{+}CD8^{+}$ or $CD45^{+}CD90.2^{+}CD4^{+}$. n = 6 mice per group from 2 independent experiments. Statistics: 2-way ANOVA with Bonferroni post-test. Error bars: SEM. **(B)** Quantification of effector function by granzyme B expression. Mice were treated in vivo with Brefeldin A for 4 hours prior to harvest to block secretion. Cells were gated on CD45+CD8+Granzyme B+. Granzyme B expression was measured by normalized MFI. n = 8 mice per group from 4 independent experiments. Error bars: SEM. Statistics performed on the non-normalized MFI values using a Mann-Whitney test.

Figure 7: Mertk signaling prevents rapid T1D progression in mice and Mertk-expressing cells are increased in the remaining insulin-containing islets of T1D patients. (A-B) NOD female mice over 20 weeks of age or WT C57BL/6 female mice were treated orally twice daily with 30mg/kg UNC2025 or saline Vehicle twice daily for **(A)** 16 hours or **(B)** 14 days. **(A)** Quantification of islet infiltration following Mertk inhibition. Whole pancreata were isolated and fixed prior to sectioning and staining. Sections were scored blindly for islet infiltration using the standard insulitis scale of 0 = uninfiltrated islet to 4 = completely destroyed islet. n=45 islets per condition from 5-6 mice per group from 2 independent experiments. Statistics: Student's T test of islet scores. **(B)** Diabetes incidence with Mertk inhibition. Mice were monitored daily for blood glucose values. Mice with two consecutive blood glucose readings of >250 mg/dL were considered to be diabetic. n = 6-14 mice per group from 4 independent experiments. Statistics: Mantel-Cox Test. **(C-D)** Immunofluorescent staining of pancreas sections from type 1 diabetes patient and control donors. **(C)** Representative images of Mertk staining (green), insulin staining (red), and tissue autofluorescence (blue). The dotted line indicates the islet border. **(D)** Blinded quantification of Mertk-expressing cell number per islet section. n= 5 patients and 4 controls.

Approximately 10 insulin-containing islets were imaged per donor. Error bars = SEM. Statistics: Two-tailed Student t test.

Movie Legends:

Movie 1: CD11c+ cells in the islets prevent T cell arrest. NOD.CD11c-DTR bone marrow (BM) chimeras containing 90% NOD.CD11c-DTR BM +10% NOD.CD11c-DTR.8.3.CD2-dsRed BM were treated twice with PBS (Intact) or DT (CD11c depleted). 48h post-treatment initiation, T cell motility was analyzed in explanted islets by 2-photon microscopy. Representative islet movies from PBS control or DT treated mice with 10 minute tracks of motion. Dashed line depicts islet border. Time (min:sec); scale bar= 50µm.

Movie 2: Mertk signaling drives regulation of T cell arrest and interactions with APCs in the islets. Activated 8.3 CD8 T cells and BDC-2.5 CD4 T cells were fluorescently labeled and co-transferred into female NOD.CD11c-mCherry mice. Mice were treated twice daily with saline vehicle or 30 mg/kg UNC2025, a small molecule inhibitor of Mertk and Flt3. 17h following the initial treatment, islets were isolated and analyzed by 2-photon microscopy. Representative islet movies from vehicle or UNC2025 treated mice with 10 minute tracks of motion. Dashed line depicts islet border. Time (min:sec); scale bar= 50µm.

Movie 3: Islet antigen-specific T cells in Mertk-/- islets show decreased motility and increased T cell arrest. Activated BDC-2.5 CD4 T cells were transferred into NOD or NOD.Mertk-/- female mice to initiate islet infiltration. Fluorescently labeled activated 8.3 CD8 and BDC-2.5 CD4 T cells were then transferred into the same mice 3-6 days later. Twenty-four hours after fluorescent T cell transfer, islets were isolated and analyzed by 2-photon microscopy. Representative islet movies from WT NOD or NOD.Mertk-/- mice with 10 minute tracks of motion. Dashed line depicts islet border. Time (min:sec); scale bar= 50µm.

Movie 4: Mertk signaling prevents T cell arrest in a solid tumor model. B78ChOva tumor cells were implanted in C57BL/6 or C57BL/6.Mertk-/- mice. Activated OT-I.Ub-GFP CD8 T cells were then transferred into tumor bearing mice mice 4-6 days later. Five to seven days after fluorescent T cell transfer, mice were treated with UNC2025 or vehicle. 18h after treatment, tumors were excised and analyzed by 2-photon microscopy. Representative movies of OT-I T cell (green) motility on the tumor surface with 10 minute tracks of motion. Collagen (blue) delineates the tumor surface.

Figure 1: CD11c+ cells in the islets prevent T cell arrest.

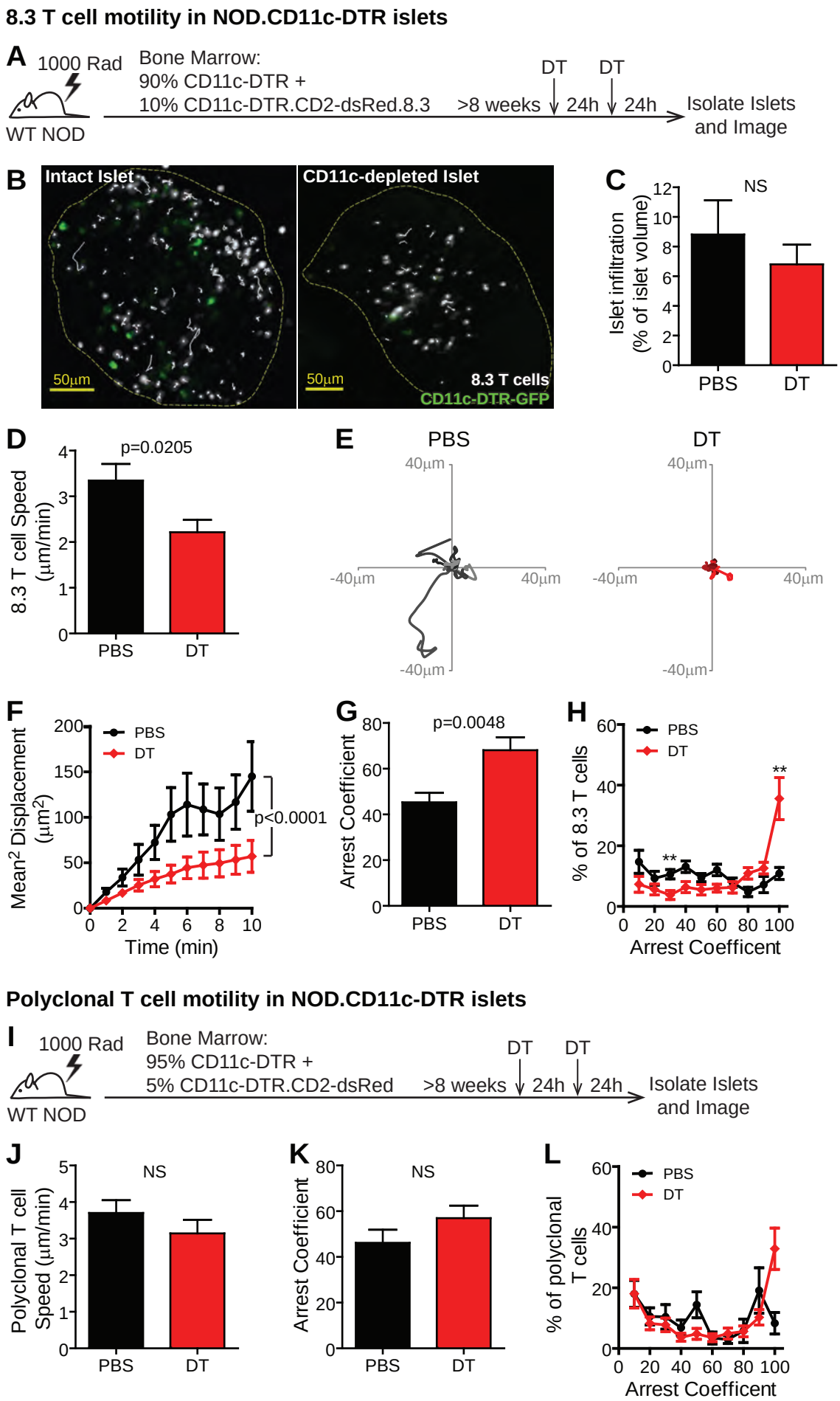

Figure 2: MerTK expressing cells increase with progression of islet infiltration.

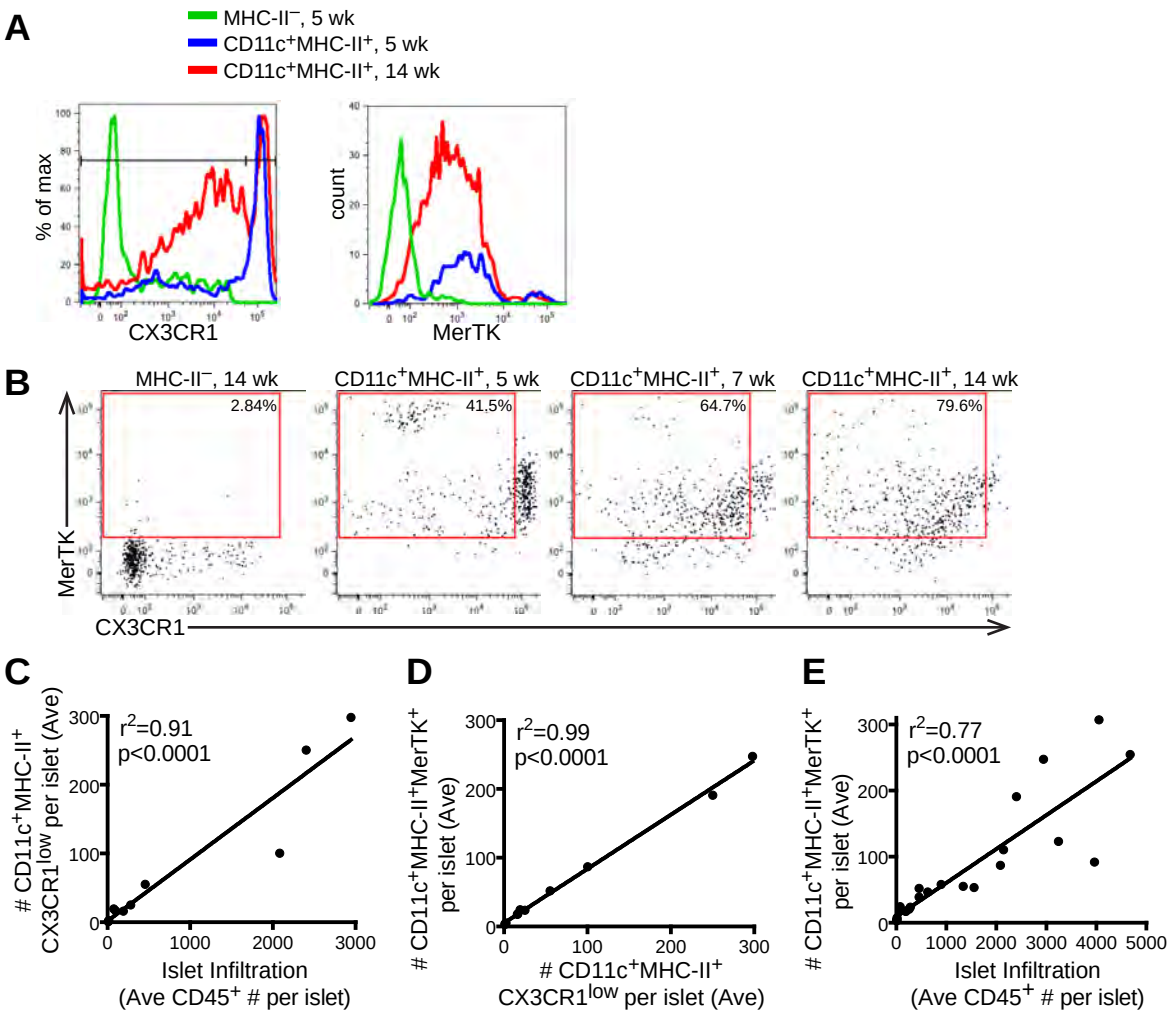

Figure 3: Mertk signaling drives suppression of T cell arrest and interactions with APCs in the islets.

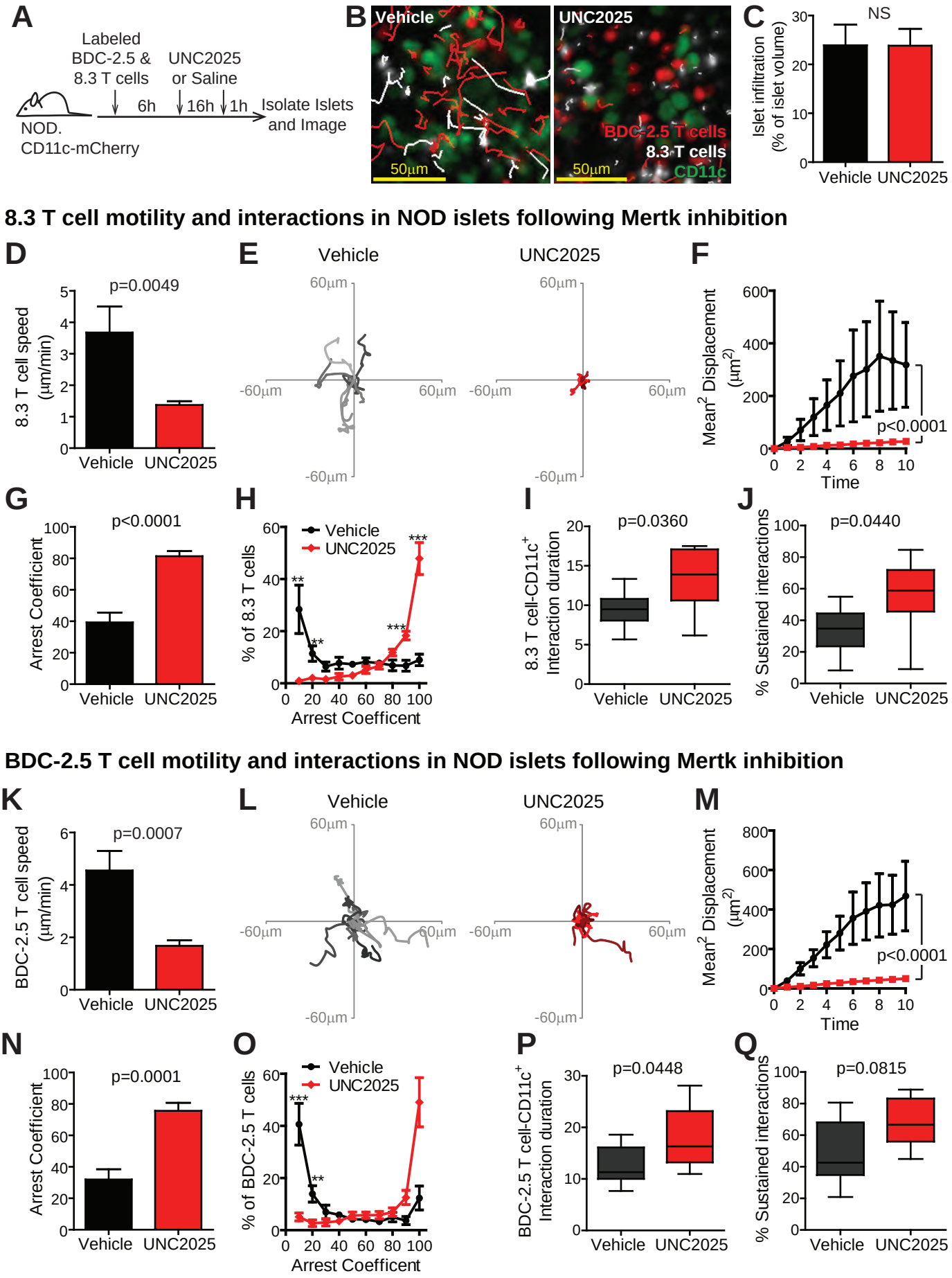

Figure 4: Islet antigen-specific T cells in Mertk-/- islets show decreased motility and increase T cell arrest.

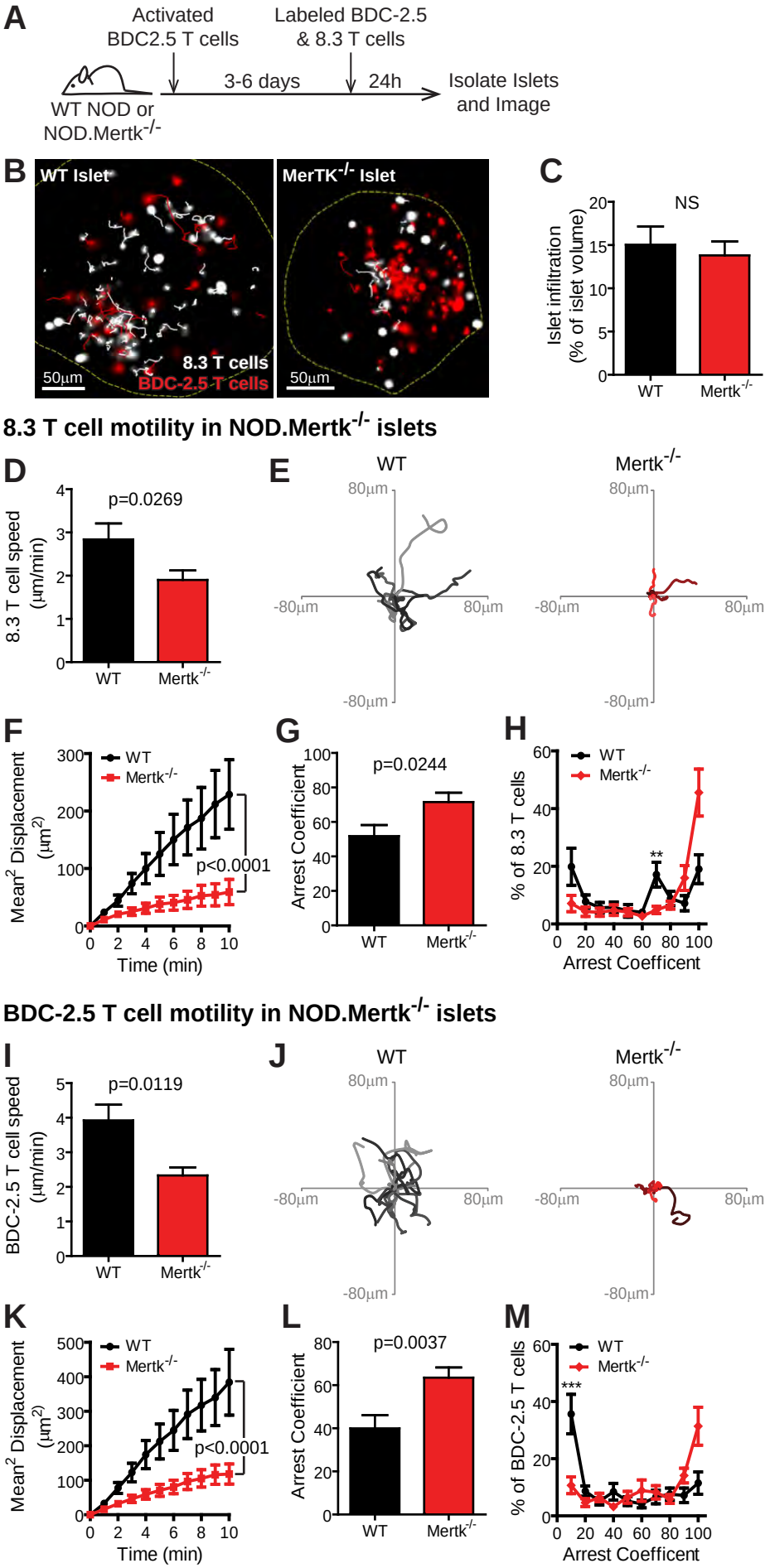

Figure 5: Mertk signaling prevents T cell arrest in a solid tumor model

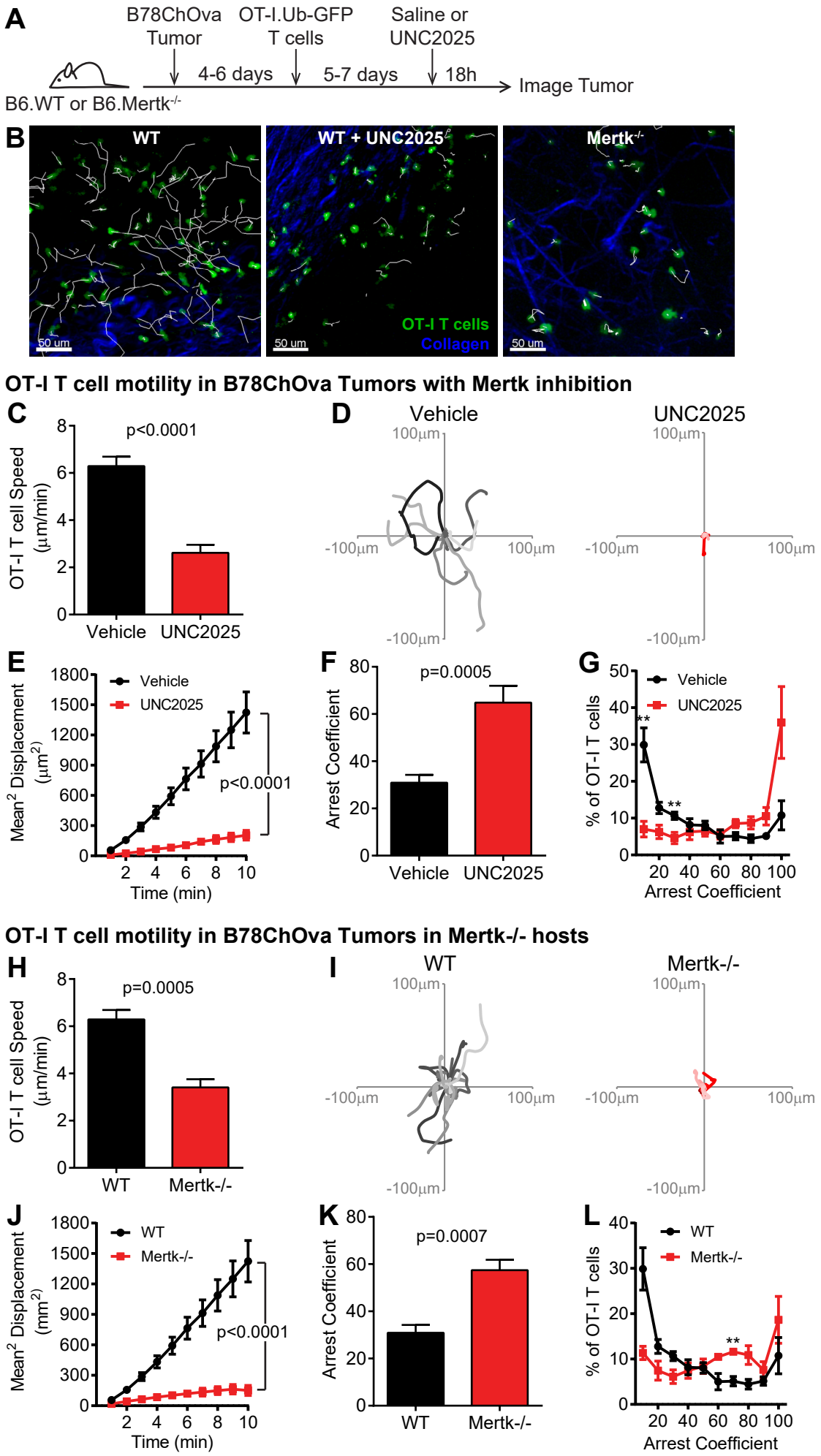

Figure 6: T cell antigen experience and effector function increases specifically at the disease site in the islets following Mertk inhibition.

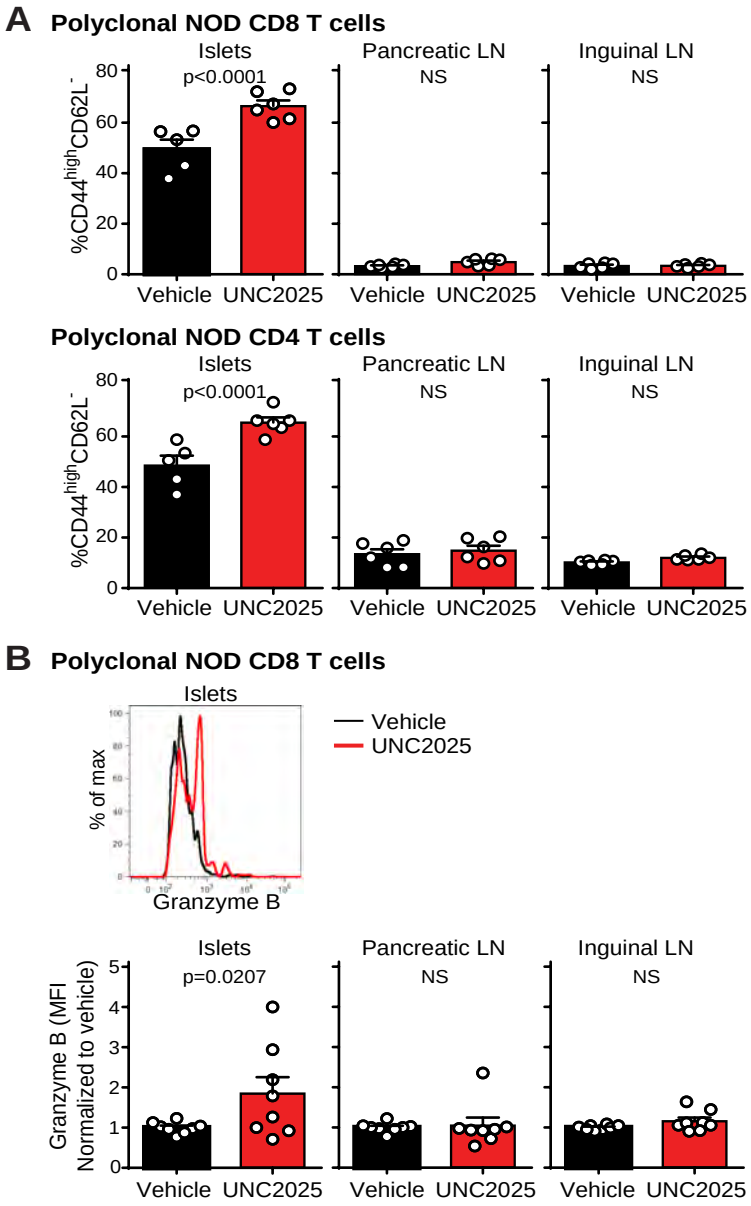
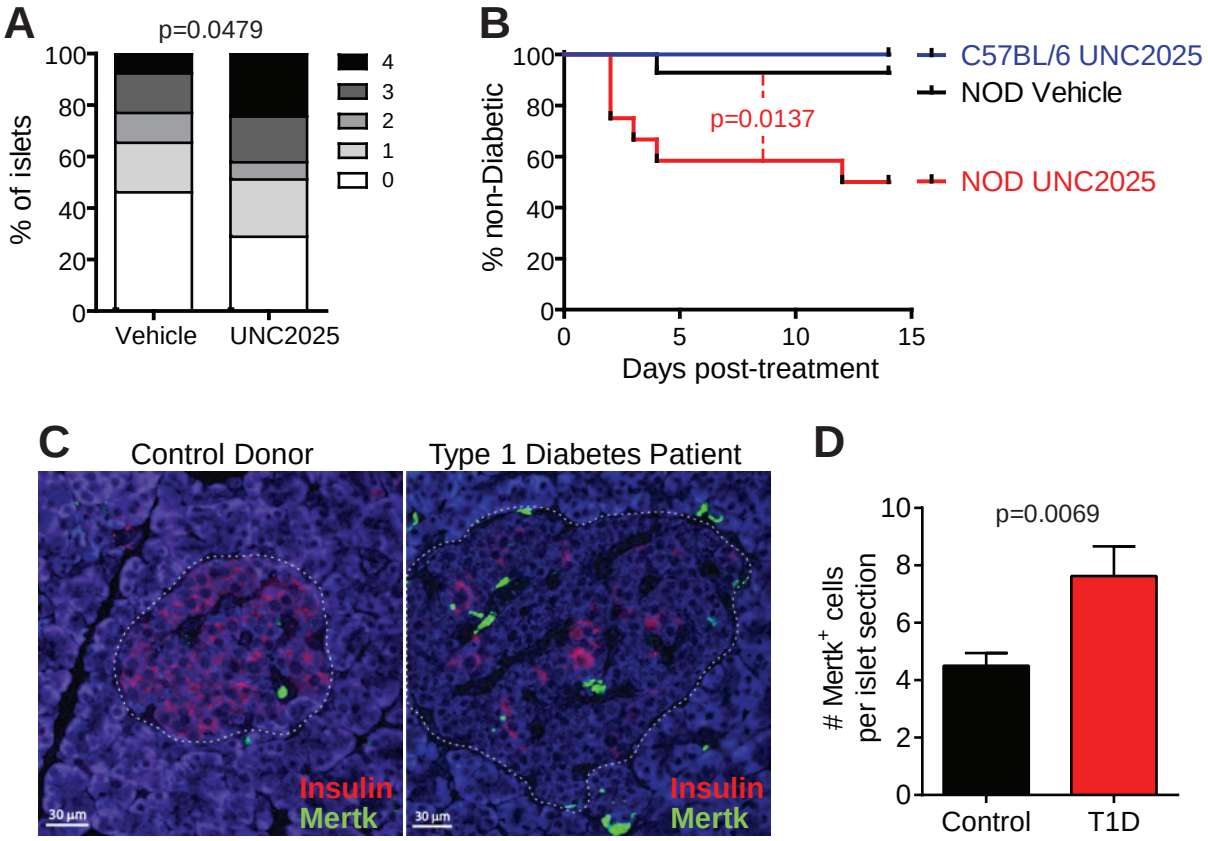
Figure 7: Mertk signaling prevents rapid T1D progression in mice and Mertk-expressing cells are increased in the remaining insulin-containing islets of T1D patients.